Mechanisms to buffer variability in cell regulation motifs close to criticality

Daniele Proverbio[1,2],* Arthur N. Montanari[1], Alexander Skupin[1,3,4], and Jorge Gonçalves[1,5]
1- Luxembourg Centre for Systems Biomedicine, University of Luxembourg, 6 Avenue du Swing, 4367, Belvaux, Luxembourg
2- College of Engineering, Mathematics and Physical Sciences, University of Exeter, EX4 4QL, Exeter, UK
3- Department of Physics and Material Science, University of Luxembourg, 162a Avenue de la Faiencerie, 1511 Luxembourg, Luxembourg
4- Department of Neuroscience, University of California San Diego, 9500 Gilman Drive, La Jolla, CA, United States and
5- Department of Plant Sciences, University of Cambridge, CB2 3EA, Cambridge, UK
(Dated: June 28, 2022)

Bistable biological regulatory systems need to cope with stochastic noise to fine-tune their function close to bifurcation points. Here, we study stability properties of this regime in generic systems to demonstrate that cooperative interactions buffer system variability, hampering noise-induced regime shifts. Our analysis also shows that, in the considered cooperativity range, impending regime shifts can be generically detected by statistical early warning signals from distributional data. Our generic framework, based on minimal models, can be used to extract robustness and variability properties of more complex models and empirical data close to criticality.

Many biological systems self-regulate their functions through bistable circuits. In particular, positive feedback loops have long been studied in systems and synthetic biology [1–3]; they regulate crucial functions like enzymatic activity or gene transcriptional changes during cell fate decisions [4, 5]. Autoactivating positive feedback loops, simple circuit motifs promoting bistability and fine regulation of dynamical states close to self-organised criticality, are of particular importance [6, 7]. Cellular heterogeneity, *i.e.*, random cell-to-cell variations [8], can further direct transitions [9, 10] and induce regime shifts between alternative stable states of gene expression or of protein concentrations [11]. Stochastic positive feedback loops have been observed in a variety of system including the transcription network of *E. coli* [12] or in the regulation of *β-galactosidase* [13], which results from a sudden transition from low ("off") to high ("on") level states of the *lac operon* at a critical point of an inducer concentration.

Close to criticality, the dynamical motif has reduced resilience and the system can exhibit augmented variability in response to noise [14, 15]. This is typical of nonlinear systems approaching a critical bifurcation and corresponds to augmented sensitivity to random perturbations and diverging response time, a phenomenon known as critical slowing down (CSD) [16, 17]. Mechanisms to buffer variability while maintaining the critical state are thus necessary to finely regulate desired transitions [13] or to better cope with undesired shifts [18].

In mono-stable systems, noise can be bound by the action of molecular compounds like microRNAs [19] as well as by temporal relays of signalling molecules [20, 21]. For critical regimes in bistable processes, a key mechanism to buffer variability is identified here: the cooperative interactions tuning the activation function of positive feedback loops. This effect can be analysed by considering the simple and well-known adimensional model for stochastic autoactivating positive feedbacks [22, 23]:

$$\dot{x} = K + c\frac{x^n}{1+x^n} - x + \eta(t)\ . \tag{1}$$

This model describes the protein concentration dynamics after RNA transcription (Supplementary Fig. S1) by a Michaelis-Menten kinetics [10, 24], where x represents the protein concentration, with steady state $\tilde{x}$ ($\dot{x}|_{\tilde{x}} = 0$), K is the basal expression rate, and c is the maximum production rate. The dissociation constant in the denominator of the Hill function was normalised to 1 without loss of generality [25]. The noise term $\eta(t)$ accounts for intrinsic stochasticity of biological processes [26]. Here, we consider additive Gaussian white noise reflecting the fast degrees of freedom in a mean field regime [27], with the statistical properties $\langle\eta\rangle = 0$, $\langle\eta(t)\eta(t')\rangle = 2\sigma\delta(t-t')$, where σ represents the noise intensity. The Hill coefficient n, which describes the nonlinear cooperative binding mechanisms, is usually interpreted as the number of transcription factors that cooperatively promote transcription [22]. The smallest value inducing bistability in the circuit is $n = 2$, while $n \to \infty$ yields the logic approximation for the activating Hill function,

$$\lim_{n\to\infty} \frac{x^n}{1+x^n} = \Theta(x-1)\,, \tag{2}$$

where $\Theta(\cdot)$ is the Heaviside step function that turns system (1) into a perfect toggle without bistability nor CSD.

This Letter investigates the dependence of resilience properties [28] on intermediate values of the cooperativity index n. As shown in Fig. 1, increasing n from 2 yields different bifurcation diagrams, where critical points shift to the left and the distance between the upper stable manifold and the unstable manifold decreases when the system gets close to criticality. We focus on systems residing on the upper branch (to be consistent with the mean field assumption) and moving left towards the

* daniele.proverbio@uni.lu

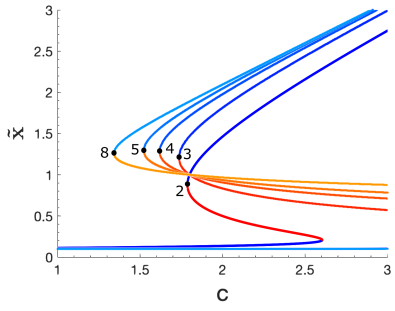

FIG. 1. Bifurcation diagrams $(\tilde{x}, c)$ of Eq. (1) for different Hill coefficients n. Stable and unstable branches are represented by blue and red colors, respectively. Black dots identify the bifurcation (saddle-node) points c_0. Each value of n is displayed close to its corresponding diagram.

saddle-node bifurcation point. This way, we investigate how biological circuits can buffer variability close to critical states by exploiting dynamical mechanisms. We also assess the parameter range where CSD-based early warning signals correctly indicate impending regime shifts.

To characterise the system stability properties, we analyse the stationary potentials and probability density functions (PDF) depending on n, in analogy to previous works [29, 30]. Consider the forward Fokker-Plank equation for the probability density function $P(x,t)$ associated with Eq. (1):

$$\frac{\partial P(x,t)}{\partial t} = -\frac{\partial}{\partial x}\left[f(x)P(x,t)\right] + \frac{\partial^2}{\partial x^2}\left[\sigma P(x,t)\right], \quad (3)$$

where $f(x)$ lumps the deterministic terms of Eq. (1). The stationary solution $P_s(x)$ takes the form [31]

$$P_s(x) = N_c e^{-\phi(x)}, \quad (4)$$

$$\phi(x) = \frac{1}{2}\ln\sigma - \frac{1}{\sigma}\int^x f(x')dx', \quad (5)$$

where $\phi(x)$ describes the adjoint stochastic potential whose depth is related to system resilience, *i.e.*, its ability to recover after a perturbation. N_c is a normalization constant such that $\int_\Omega P_s(x) = 1$ (Ω is the domain).

Fig. 2 shows the dependency of $\phi(x)$ and $P_s(x)$ on n when the system is either in an "off" state far away from criticality (Fig. 2a,b), close to the criticality (Fig. 2c,d) or beyond it, in an "on" state (Fig. 2e,f). Increasing the cooperativity index n does not alter the underlying bistability, but modifies the depth of the potential and increases the separation of alternative states (Supplementary Fig. S2). For the "off" and "on" states, the corresponding equilibria exhibit significantly deep attractor basins with only minor dependence on n, as also indicated in the bifurcation diagrams (Fig. 1) and by $P_s(x)$. Close to critical points, the picture changes. The potential $\phi(x)$ displays two wells, which are more evident and symmetric for larger n, suggesting that both states

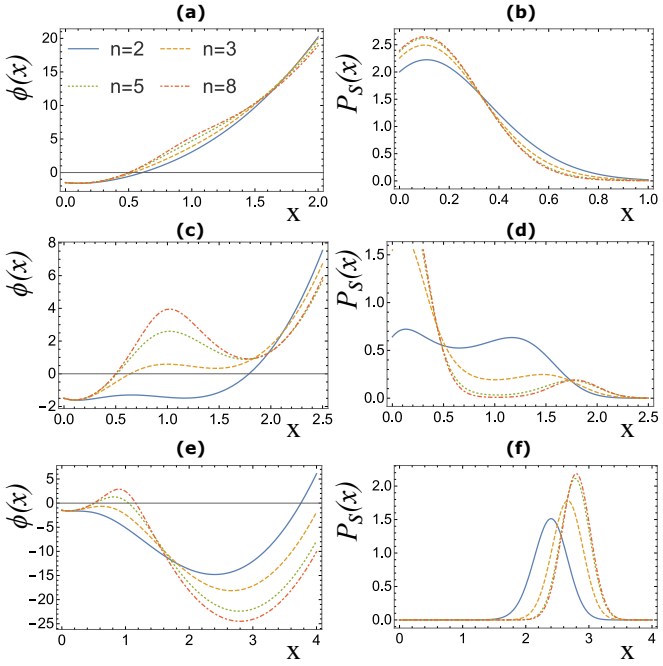

FIG. 2. Effect of the Hill coefficient n on the stochastic potential $\phi(x)$ (left column) and on the stationary probability density function $P_s(x)$ (right column), when only additive white noise is present. (a, b) $c = 0.8$ ("off" state); (c, d) $c = c_0(n) + 0.05$ (multistable region); (e, f) $c = 2.7$ ("on" state favoured). In all cases, $K = 0.1$ and $\sigma = 0.05$.

become equally occupied in noisy environments. For increasing n, $P_s(x)$ displays sharper peak separation between the bistable states: the system diffuses less to intermediate states and is more constrained around single equilibrium values, as anticipated due the steeper potential barriers in $\phi(x)$. Random deviations are thus suppressed faster and transitions from one state to another are sharper and are therefore more robust against noise.

We close investigate how n influences variability measures, like variance and autocorrelation, close to criticality. Obtaining globally analytic expressions is challenging, in particular for high values of n. Hence, we focus on a local analysis close to the bifurcation points and employ a geometrical methodology. To derive generic results for critical manifolds, we use their local topological equivalence to bifurcation normal forms [32]. For saddle-node bifurcations like in Fig. 1, the associated normal form is

$$\dot{x} = p - x^2, \quad (6)$$

with two equilibrium manifolds $\tilde{x}_{1,2} = \pm\sqrt{p}$, one stable (+) and the other unstable (−). Note that the normal form corresponds to a parabola. To study the behaviour of stochastic solutions near the stable manifold, consider the evolution of its first-order perturbation, $y = \delta x|_{\tilde{x}_1}$ exposed to the same additive white noise $\eta(t)$ as in Eq. (1) [33]. Since $k = 2\sqrt{p}$ is the distance of the control parameter value from its critical value $p_0 = 0$, note that k is proportional to $c - c_0$ from the original system, follow-

ing normal form properties. The corresponding Langevin equation accounting for mean field fluctuations around the stable equilibrium is then given by

$$\dot{y} = -ky + \eta(t)\,. \tag{7}$$

Eq. (7) is a typical Ornstein–Uhlenbeck (OU) process with exact solutions for statistical moments [31].

To connect the quantitative effects of n with the more qualitative topological form in Eq. (6), recall that n widens or narrows the local parabolic shape of the original bifurcation diagram for Eq. (1) (Fig. 1). From basic geometric considerations, Eq. (6) thus needs to be augmented with a term ρ to modify the focal width of its parabolic stable manifold, which corresponds to the width of the parabola at the focal level. This leads to

$$\dot{x} = p - \rho x^2\,. \tag{8}$$

In this formulation, ρ corresponds to the focal width of the normal form. Supplementary Material contains analytical derivations for the approximation of system (1) to the normal form (8), and its relationships with the geometrical results. Propagating ρ into Eq. (7) adds a tuning term to the bifurcation parameter, $k \to \sqrt{\rho}k$. Hence, the corresponding OU process for a semi-quantitative saddle-node normal form is

$$\dot{y} = -\sqrt{\rho}ky + \eta(t)\,. \tag{9}$$

Among its statistical moments and power spectral properties, we are primarily interested in quasi-steady-state variance (Var) and lag-1 autocorrelation (AC1), measures of system variability close to criticality. They have been proposed as proxies for system resilience and early warning signals (EWS) of impending bifurcation points [18, 34]. Based on our mapping to the OU process (Eq. (9)), the analytical solutions for Var and AC1 take the form [31]:

$$\mathrm{Var} = \frac{\sigma}{\sqrt{\rho}k}, \quad \mathrm{AC1} = e^{-\sqrt{\rho}k}\,. \tag{10}$$

Eqs. (10) are generic for noisy saddle-node bifurcations. Fig. 3a,b shows them as functions of ρ and k. To connect with the original autoactivating feedback system, we estimate the focal width of the bifurcation diagrams for each n by fitting a parabolic form $c = \alpha\tilde{x}^2 + \beta\tilde{x} + \gamma$ to the data points of each bifurcation diagram in the vicinity of the saddle point. Using MATLAB Curve Fitting toolbox also provides uncertainties over $\vec{\theta} = [\alpha, \beta, \gamma]$, resulting from small deviations from a perfect parabolic shape. By definition, the fitted focal width is

$$FW = 2|\tilde{x}(c_F) - \tilde{x}_F|\,, \tag{11}$$

where $(\tilde{x}_F, c_F)$ are the coordinates of the parabolic focus. The associated standard deviation is propagated from the fitted parameter uncertainties $\mathrm{std}(\bar{\theta}_i)$ as

$$\mathrm{std}(FW) = \left[\sum_i \left(\frac{\partial FW}{\partial \theta_i}\mathrm{std}(\theta_i)\right)^2\right]^{\frac{1}{2}}. \tag{12}$$

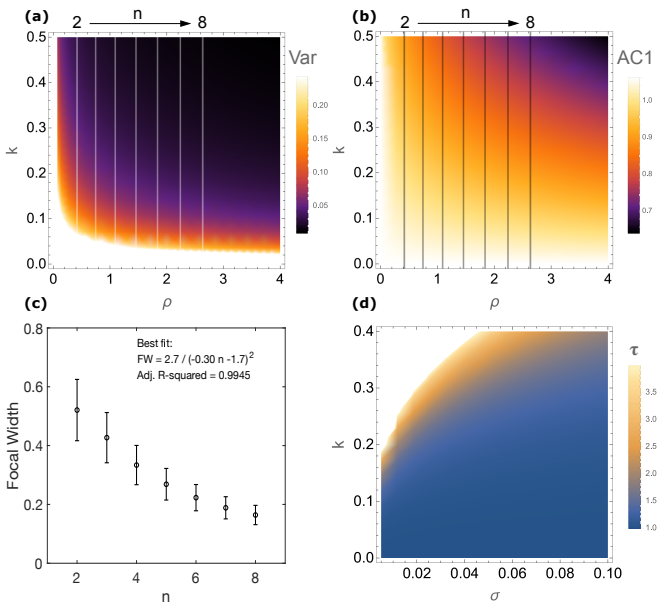

FIG. 3. Theoretical dependence of EWS measures (a) Var and (b) AC1 on ρ (related to focal width) and k (distance measure from critical parameter values). Vertical lines represent slices for fixed values of $\hat{\rho}$ (Eq. (13)) corresponding to the mean FW shown in panel c. The associated n values increase from left to right. (c) Relationship between FW (Eq. (11)) and corresponding values of n, with best fit. Error bars correspond to one standard deviation (Eq. (12)). (d) Generic escape rate τ as a function of noise level σ and k (Eq. (15)).

The relationship between FW and n is plotted in Fig. 3c, with the corresponding $\mathrm{std}(FW)$. The pattern decreases quadratically, thereby marking a rapid decrease followed by almost plateauing. Hence, a bounded and relatively small cooperativity index is in principle sufficient to effectively buffer variability close to criticality.

The estimated $\hat{\rho}$ values from fitted focal widths, for $n = 2$ to $n = 8$, are obtained as

$$\hat{\rho} = \xi(FW)^{-1}\,, \tag{13}$$

where ξ is a tuning parameter proportional to the Hill function (Supplementary Material). Mean $\hat{\rho}$ values are marked in Fig. 3a,b with solid vertical lines. Consistently with the trend observed in Fig. 3c, the mean values spread as n increases (from left to right). Low n values yield higher sensitivity to noise, as both Var and AC1 show substantially higher values for small cooperativity indices n, even when k is large (i.e., further away from the critical point). Thus, values of ρ can either belong to two regions: a sensitive subspace nested between a region where both metrics span high values for all k (left side of Fig. 3a,b), or another one where both metrics maintain low values for most k and increase rapidly close to criticality (right side of Fig. 3a,b). The region $\hat{\rho} \to \infty$ corresponds to the idealized toggle switch model (2) with $n \to \infty$, where Var and AC1 also change abruptly in a step-wise manner. The ultra-sensitive region $\hat{\rho} \to 0$

is spanned by increasing dissociation constants (Supplementary Fig. S3), and potentially by changing other parameters, here not explicitly considered, or by different activation functions describing, for example, wild-type vs mutant organisms [26].

We finally investigate the performance of EWS against impending bifurcation points. The motivation is to consider complex systems lacking validated mechanistic models; in our case, this would translate to a scenario where n—or even the precise activation function—of an eukaryotic cell is poorly identifiable [26]. This consideration leads to questioning if we can identify statistical signals, computed on empirical data, that provide reliable information about the system's loss of resilience. Increasing trends of Var and AC1 have been widely suggested to work as EWS [18, 34] but their robustness remains elusive. To study how generic they are in the identified parameter range and to account for mean trends and uncertainties, we numerically integrate the original stochastic system (1) using the Euler-Maruyama method. To mimic cell populations slowly evolving close to equilibrium, we sample 10^4 time points over 200 repeated experiments in dependence of c. This leads to a distribution of statistical indicators (*e.g.*, see Fig. 4a, inset).

To distinguish between bifurcation-driven loss of resilience and noise-induced transitions, we measure the scale between the distance to the bifurcation point and the noise level by the Kramers escape rate $\tau = 2\pi(\sqrt{|U''(\tilde{x}_1)U''(\tilde{x}_2)|})^{-1}\exp[(U(\tilde{x}_2) - U(\tilde{x}_1))/\sigma]$ [31]. For any saddle-node bifurcation manifold (8) equipped with additive noise, $U(\tilde{x}_2) - U(\tilde{x}_1) = (4/3)(k^3/\sqrt{\rho})$ and $|U''(\tilde{x}_{1,2})| = 2\sqrt{p\rho}$. Hence,

$$\tau = \frac{\pi}{k\sqrt{\rho}}\exp\left[\frac{4}{3}\frac{k^3}{\sqrt{\rho}\sigma}\right]. \tag{14}$$

Values lying at the exponential boundary of the generic form

$$\tau \simeq \mathcal{O}(\exp[k^3/\sigma]) \tag{15}$$

(Fig. 3d) provide comparable ranges of control parameters and noise levels for all simulations with different n. They distinguish two regimes, one where few noise-induced transitions might occur ($\tau \lesssim 2$, Fig. 4a,b) and another regime primarily determined by bifurcation-driven resilience loss ($\tau \gtrsim 2$, Fig. 4c,d). For the considered $\sigma = 0.02$, the system is very close to critical points.

Fig. 4a–d display average values for Var and AC1 from numerical simulations. When the dynamics is mostly characterised by the bifurcation (Fig. 4c,d), both measures display patterns consistent with those predicted in Fig. 3a,b and increasing n better buffers variability. When the noise level becomes comparable to the potential depths (Fig. 2c,d), Vars for different n become very close to each other due to the more prominent role of noise-induced uncertainties. By contrast, AC1s (Fig. 4a,b) remain separated due to their lower sensitivity to noise (*cf.* Eq. (10)), but with less marked—and, therefore, harder-to-detect—trends, similarly to those observed in real-world data [35].

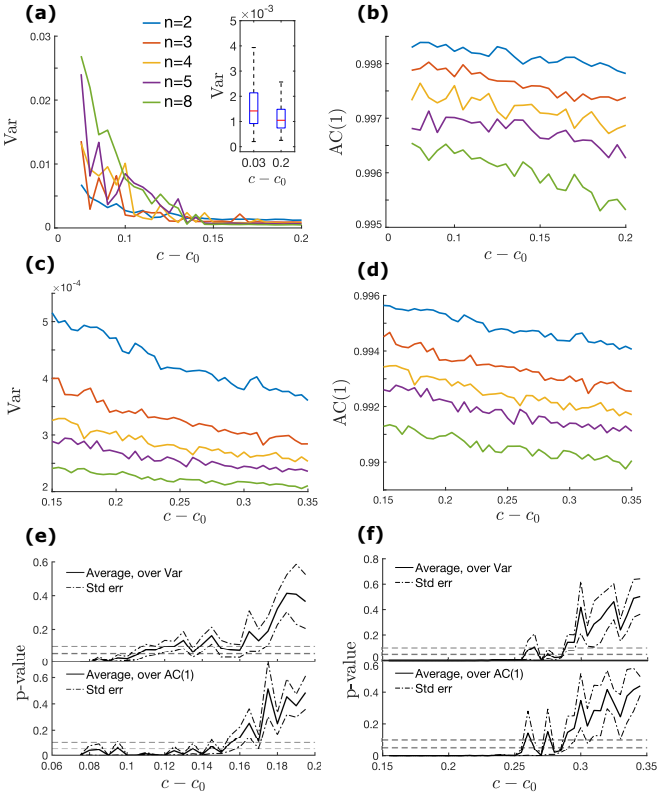

FIG. 4. Average trends of (a) Var and (b) AC1 as a function of c close to bifurcation c_0, in the regime where noise-induced transitions might occur (blue area of Fig. 3d). Simulations are presented over 200 realizations for different n. For each c, the indicators spread into distributions, as exemplified for two c values in inset (a). (c,d) Average trends of Var and AC1 farther from bifurcation c_0. (e,f) Evolution of p-values between Var and AC1 distributions at each $c - c_0$ and the "basal" distribution. The "basal" distribution corresponds to (e) $c - c_0 = 0.2$ (starting "closer to bifurcation") and (f) $c - c_0 = 0.35$ ("farther from bifurcation"). Dashed lines represent typically used p-values in biological experiments.

To quantify significant increasing trends as EWS, we assess significant p-values between the computed distributions close to criticality and those far from the bifurcation ("basal") (inset in Fig. 4a). Fig. 4e,f show patterns of p-values from Var and AC1, averaged over all n. The p-values are computed closer to the bifurcation in Fig. 4e ($c - c_0$ corresponding to the parameters in Fig. 4a,b) and farther from the bifurcation in Fig. 4f ($c - c_0$ corresponding to the parameters in Fig. 4c,d). Closer values maintain p-value < 0.01. This analysis certifies the potential use of proposed EWS to detect approaching bifurcation points in biological motifs, providing a quantification of how much in advance the EWS become significant depending on the reference ("basal") and on the p-values threshold (dashed lines in Fig. 4e,f).

Our study characterised fundamental dynamical mech-

anisms to buffer systems' variability in critical regimes. We determined parameter ranges, corresponding to plausible cooperativity values for the positive feedback loop motif, where both variance and autocorrelation display low relative sensitivity to additive noise. In other ranges, however, the system poorly buffers its variability. Investigating whether these ranges could correspond to other dynamical mechanisms is demanded for future studies, along with the investigation of the effect of multiplicative noise. These may unravel alternative ways by which cells regulate their states or support the hypothesis of a self-organised fine-tuning in "safe" parameter spaces. Overall, our analysis contributes with quantitative insights to analytical and experimental studies of bistable systems' resilience and allows connecting general and system-specific predictions [28].

We also assessed the sensitivity of proposed EWS to regulation mechanisms. As several indicators have been developed upon to detect cell-fate decisions [14] and to possibly anticipate undesired shifts to, *e.g.*, cancerous states [36, 37], our results constitute an important step to interpret and apply them correctly. In the considered parameters' range, they are sufficiently generic to detect resilience loss. However, their use should be treated carefully if other quantitative mechanisms between noise and bifurcations might be at play, possibly shadowing theoretical trends. Following our methodology, future studies might inquire other indicators and their behaviour under changing n and additional conditions. Our framework can also be easily extended to inquire the performance of buffers and EWS in different dynamical models and experimental setups.

The authors thank J. Fuentes for valuable discussions. D.P. is supported by the Luxembourg National Research Fund (FNR) PRIDE DTU CriTiCS (10907093) and A.S. by the FNR (C14/BM/7975668/CaSCAD) and by the NIH NBCR (NIH P41 GM103426).

[1] L. De Mot, D. Gonze, S. Bessonnard, C. Chazaud, A. Goldbeter, and G. Dupont, Biophys. J. **110**, 710 (2016).
[2] M. Acar, A. Becskei, and A. Van Oudenaarden, Nature **435**, 228 (2005).
[3] M. T. Guinn, Y. Wan, S. Levovitz, D. Yang, M. R. Rosner, and G. Balázsi, Front. Genet. **11**, 1292 (2020).
[4] S. Huang, Y.-P. Guo, G. May, and T. Enver, Develop. Biol. **305**, 695 (2007).
[5] J. Fiorentino, M.-E. Torres-Padilla, and A. Scialdone, Ann. Rev. Gen. **54**, 167 (2020).
[6] U. Alon, *An introduction to systems biology: design principles of biological circuits* (CRC press, 2019).
[7] S. Tripathi, D. A. Kessler, and H. Levine, Phys. Rev. Lett. **125**, 088101 (2020).
[8] N. Komin and A. Skupin, Current Opinion in Systems Biology **3**, 154 (2017).
[9] M. Kaern, T. C. Elston, W. J. Blake, and J. J. Collins, Nat. Rev. Gen. **6**, 451 (2005).
[10] M. Weber and J. Buceta, PloS One **8**, e73487 (2013).
[11] P. Thomas, N. Popović, and R. Grima, P. Natl. Acad. Sci. USA **111**, 6994 (2014).
[12] R. Milo, S. Shen-Orr, S. Itzkovitz, N. Kashtan, D. Chklovskii, and U. Alon, Science **298**, 824 (2002).
[13] E. M. Ozbudak, M. Thattai, H. N. Lim, B. I. Shraiman, and A. Van Oudenaarden, Nature **427**, 737 (2004).
[14] M. Mojtahedi, A. Skupin, J. Zhou, I. G. Castaño, R. Y. Leong-Quong, H. Chang, K. Trachana, A. Giuliani, and S. Huang, PLoS Biol. **14**, e2000640 (2016).
[15] Y. Sharma, P. S. Dutta, and A. Gupta, Phys. Rev. E **93**, 032404 (2016).
[16] J. Scholz, J. Kelso, and G. Schöner, Phys. Lett. A **123**, 390 (1987).
[17] T. A. Byrd, A. Erez, R. M. Vogel, C. Peterson, M. Vennettilli, G. Altan-Bonnet, and A. Mugler, Phys. Rev. E **100**, 022415 (2019).
[18] M. Scheffer, J. Bascompte, W. A. Brock, V. Brovkin, and S. R. e. a. Carpenter, Nature **461**, 53 (2009).
[19] V. Siciliano, I. Garzilli, C. Fracassi, S. Criscuolo, S. Ventre, and D. Di Bernardo, Nat. Commun. **4**, 1 (2013).
[20] I. Lestas, G. Vinnicombe, and J. Paulsson, Nature **467**, 174 (2010).
[21] D. Del Vecchio, A. J. Dy, and Y. Qian, Journal of The Royal Society Interface **13**, 20160380 (2016).
[22] M. Santillán, Math. Mod. Nat. Phen. **3**, 85 (2008).
[23] S. H. Strogatz, *Nonlinear dynamics and chaos* (CRC press, 2018).
[24] D. Frigola, L. Casanellas, J. M. Sancho, and M. Ibañes, PloS One **7**, e31407 (2012).
[25] P. Smolen, D. A. Baxter, and J. H. Byrne, Am. J. Physiol.-Cell Ph. **274**, C531 (1998).
[26] J. Hasty, J. Pradines, M. Dolnik, and J. J. Collins, P. Natl. Acad. Sci. USA **97**, 2075 (2000).
[27] N. Berglund and B. Gentz, *Noise-induced phenomena in slow-fast dynamical systems: a sample-paths approach* (Springer Science & Business Media, 2006).
[28] L. Dai, K. S. Korolev, and J. Gore, P. Natl. Acad. Sci. USA **112**, 10056 (2015).
[29] N. Friedman, L. Cai, and X. S. Xie, Phys. Rev. Lett. **97**, 168302 (2006).
[30] N. Kumar, T. Platini, and R. V. Kulkarni, Phys. Rev. Lett. **113**, 268105 (2014).
[31] C. W. Gardiner, *Handbook of Stochastic Methods* (Springer, Boca Raton, 1985).
[32] C. Kuehn and C. Bick, Sci. Adv. **7**, eabe3824 (2021).
[33] C. Kuehn, Physica D **240**, 1020 (2011).
[34] C. Trefois, P. M. Antony, J. Goncalves, A. Skupin, and R. Balling, Curr. Opin. Biotech. **34**, 48 (2015).
[35] D. Proverbio, F. Kemp, S. Magni, and J. Gonçalves, PLOS Computational Biology **18**, e1009958 (2022).
[36] B. Yang, M. Li, W. Tang, W. Liu, S. Zhang, L. Chen, and J. Xia, Nat. Commun. **9**, 1 (2018).
[37] K. Aihara, R. Liu, K. Koizumi, X. Liu, and L. Chen, Gene **808**, 145997 (2022).